RESEARCH ARTICLE

Effects of membrane potentials on the electroporation of giant unilamellar vesicles

Md. Abdul Wadud[1]*, Mohammad Abu Sayem Karal[1]*, Md. Moniruzzaman[1], Md. Mamun Or Rashid[2]

1 Department of Physics, Bangladesh University of Engineering and Technology, Dhaka, Bangladesh,
2 Department of Pharmacy, Noakhali Science and Technology University, Noakhali, Bangladesh

* asayem221@phy.buet.ac.bd (MASK); mdabdulwadud.140722@s.pust.ac.bd (MAW)

Abstract

Living organisms maintain a resting membrane potential, which plays an important role in various biophysical and biological processes. In the context of medical applications, irreversible electroporation (IRE) is a non-thermal and minimally invasive technique that utilizes precisely controlled electric field pulses of micro- to millisecond durations to effectively ablate cancer and tumor cells. Previous studies on IRE-induced rupture of cell-mimetic giant unilamellar vesicles (GUVs) have primarily been conducted in the absence of membrane potentials. In this study, we investigated the electroporation of GUVs, including parameters such as the rate constant of rupture and the probability of rupture, in the presence of various negative membrane potentials. The membranes of GUVs were prepared using lipids and channel forming proteins. As the membrane potential increased from 0 to −90 mV, the rate constant of rupture showed a significant increase from $(7.5 \pm 1.6)\times10^{-3}$ to $(35.6 \pm 5.5)\times10^{-3}$ s^{-1}. The corresponding probability of rupture also exhibited a notable increase from 0.40 ± 0.05 to 0.68 ± 0.05. To estimate the pore edge tension, the electric tension-dependent logarithm of the rate constant was fitted with the Arrhenius equation for different membrane potentials. The presence of membrane potential did not lead to any significant changes in the pore edge tension. The increase in electroporation is reasonably explained by the decrease in the prepore free energy barrier. The choice of buffer used in GUVs can significantly influence the kinetics of electroporation. This study provides valuable insights that can contribute to the application of electroporation techniques in the biomedical field.

Citation: Wadud M.A, Karal MAS, Moniruzzaman M., Rashid M.MO (2023) Effects of membrane potentials on the electroporation of giant unilamellar vesicles. PLoS ONE 18(9): e0291496. https://doi.org/10.1371/journal.pone.0291496

Editor: Jian Xu, East China Normal University School of Life Sciences, CHINA

Received: June 14, 2023

Accepted: August 31, 2023

Published: September 12, 2023

Data Availability Statement: All relevant data are within the paper.

Funding: This work was supported partly by the Special allocation, Ministry of Science and Technology, Bangladesh (39.00.0000.009.99.024.22-901), Grant of Advanced Research in Education, Ministry of Education, Bangladesh (37.20.0000.004.033.020.2022 (part 4)-596), and Basic Research Grant of Bangladesh University of Engineering and Technology (Est/R-60/Re-5336). The funders had no role in study design, data

1. Introduction

The electrochemical potential difference between the intracellular and extracellular environments gives rise to a membrane potential (φ_m) that spans a range of −20 to −150 mV [1]. This negative membrane potential plays a crucial role in various cellular processes [2], which include regulating cell proliferation and differentiation [3,4]. It exerts a regulatory influence on the dynamics of phospholipids in the plasma membrane as well as on K-Ras signaling [5]. It also plays a pivotal role in shaping the regulation of dopamine transporter trafficking at the plasma membrane [6].

collection, and analysis, the decision to publish, or preparation of the manuscript. There was no additional external funding received for this study.

Competing interests: The authors have declared that no competing interests exist.

On the other hand, irreversible electroporation (IRE) is an advanced technique utilized for tissue and cancer cell ablation [7,8]. In this technique, a high-intensity electric field is applied to cells to induce the opening of membrane pores, resulting in a sudden and significant increase in membrane permeability. This technique has gained recognition and is being explored for various medical applications, including the treatment of different types of cancer [9]. It has been well-known that the structure of the cell membrane is highly intricate, and accurately studying the changes in its various components and quantities poses significant challenges [10]. As a result, researchers often rely on mimics of cell membranes, such as lipid membranes formed in vesicles. Giant unilamellar vesicles (GUVs) with sizes comparable to cells have been extensively utilized in numerous experiments [11]. These vesicles provide a convenient model system that allows for real-time observations using optical microscopes. By employing GUVs, researchers gain valuable insights into the behavior and properties of cell membranes under controlled conditions.

When an external electric field is applied, it generates lateral electric tension (σ_e) in the lipid membranes of vesicles. If this tension surpasses a critical threshold, membrane poration occurs, ultimately leading to ablation or cell death. Similarly, mechanical tension (σ_m) can be induced in membranes by applying suction pressure using a micropipette [12]. This technique allows for the controlled manipulation and study of membrane mechanics. Recently, several experiments have been conducted using σ_e and σ_m to investigate the effects of varying lipid composition, surface charge density, cholesterol concentration, and osmotic pressure in the absence of φ_m [13]. These studies aim to understand the impact of these parameters on the kinetics of GUVs and their rupture probability. In living cells, resting membrane potential is maintained across the cell membrane, which is essential for various cellular processes. By studying the effects of different membrane potentials on electric field-induced rupture, researchers aim to gain insights into the mechanisms underlying the response of cells and vesicles to electric fields.

Membrane proteins play crucial roles in essential processes for the survival and function of biological cells. They are involved in mediating the transport of ions and larger solutes across membranes, facilitating communication between the cell and its surroundings through receptors, and catalyzing chemical reactions as membrane-embedded enzymes [14]. In order to generate φ_m across the membranes of GUVs, a commonly employed method involves the use of a channel-forming protein called Gramicidin A (GrA) [15,16]. It is an antibiotic peptide produced by *Bacillus brevis* that forms inorganic monovalent cation-permeable channels in biological membranes and lipid bilayers. Its small size and ease of chemical modification make it an excellent candidate for investigating the properties of real ion channels, as they share similar structural features [17]. Generally, ion channels regulate ionic permeability [18], and manage the passage of ions in all excitable cell membranes [19].

Membrane potential is vital for the rapid permeabilization of the plasma membrane and lipid bilayers by the antimicrobial peptide lactoferricin B [20]. The application of membrane potentials has been found to have a significant impact on various aspects of membrane behavior, including the effects of antimicrobial peptide magainin 2-induced membrane poration as well as the binding interactions between membranes and magainin 2 [21]. The membrane potential also plays a crucial role in the entry process of lactoferricin B-derived 6-residue antimicrobial peptide and cell-penetrating peptide transportan 10 into single *Escherichia coli* cells and lipid vesicles [22].

Membrane tension is a fundamental physical parameter that presents both challenges and widespread implications in cell biology. Maintaining proper membrane tension is essential for the integrity and functionality of cells [23,24]. Osmotically induced membrane tension plays a crucial role in facilitating the triggering of electropermeabilization in living cells [25,26].

When an external force, such as electrical, mechanical, or optical tension, causes the formation of a pore in the lipid bilayer, it leads to the generation of pore edge tension (Γ) in the membrane [27–30]. The pore edge tension, also known as line tension, is a critical factor that determines the stability of pores formed in the membrane and drives their closure. This tension is intimately linked to membrane stability and has a significant impact on the mechanisms involved in membrane resealing after pore formation. It is an intrinsic characteristic of the membrane that arises from the physicochemical properties and amphiphilic nature of the lipid molecules within the bilayer. This tension reflects the energy cost per unit length required to maintain an open pore in the membrane. The increase of monolayer spontaneous curvature on tension-induced pore formation decreases the Γ, resulting in to an increase in the rupture kinetics of GUVs [31].

Cellular homeostasis relies on the maintenance of a resting membrane potential across cell membranes. Consequently, it is crucial to examine the static and dynamic behavior of cell-mimetic vesicles when exposed to an electric field in the presence of various membrane potentials. Previous studies conducted by the Yamazaki group have explored the impact of membrane potential on vesicles and cells, providing insights into the mechanisms underlying damage induced by antimicrobial peptides and cell-penetrating peptides on lipid bilayers of GUVs and cell membranes [22,32,33]. However, there has been a notable lack of investigations focused on studying the effects of membrane potential on electroporation of lipid vesicles. Therefore, the primary objective of this research is to investigate electric field-induced vesicle electroporation and measure pore edge tension under the influence of various membrane potentials. By examining multiple electroporation regimes in the presence of membrane potential, we aim to comprehensively evaluate the effects of the electric field on biological cells. The outcomes of this research will contribute to a deeper understanding of the underlying mechanisms of electroporation and provide essential information for the effective development of electroporation technique-based biomedical applications.

2. Materials and methods

2.1 Chemicals and reagents

1,2-dioleoyl-*sn*-glycero-3-phospho-(1´-*rac*-glycerol) (sodium salt) (DOPG), and 1,2-dioleoyl-*sn*-glycero-3-phosphocholine (DOPC) were purchased from Avanti Polar Lipids Inc. (Alabaster, AL). Gramicidin A (GrA) from Bacillus brevis, 4-(2-Hydroxyethyl) piperazine-1-ethanesulfonic acid (HEPES), 1,4-Piperazinediethanesulfonic acid (PIPES), Tetraethylammonium chloride (TEAC), Bovine serum albumin (BSA), and O,O´-Bis (2-aminoethyl) ethyleneglycol-*N*,*N*,*N*´,*N*´, -tetraacetic acid (EGTA), potassium chloride (KCl), sodium chloride (NaCl), glucose, and sucrose were purchased from Sigma-Aldrich (Germany).

2.2 Synthesis of GUVs

DOPG/DOPC/GrA (40/60/0.01)-GUVs, where the numbers indicate the molar ratio, were prepared using the natural swelling method [34]. To prepare the samples, we started by adding 80 μL of 1 mM DOPG and 120 μL of 1 mM DOPC, both dissolved in chloroform, into a 5 mL glass vial. After that, it was added 20 μL of 1 μM GrA, which was dissolved in ethanol, to the same vial. The DOPG, DOPC, and GrA components mixed together naturally due to their high diffusion rates in the solvent. Additionally, we gently shook the vial by hand to ensure thorough mixing. At this stage, it was allowed the mixture to sit for approximately 10 minutes. This process was repeated for another vial to prepare a total of two vials for each experiment. Then the solvents were evaporated using a gentle flow of nitrogen gas. To ensure complete drying, the glass vials were placed in a vacuum desiccator connected to a rotary vacuum pump for at least 12 hours. Next, 20 μL of MilliQ water was added to each vial, and the vials were prehydrated by incubating them at ~48˚C for 8 minutes in a mini water bath. Afterward, 1 mL of buffer A (10 mM HEPES, 150 mM KCl, pH 7.5, and 1 mM EGTA) containing 0.10 M sucrose was added to each vial. The samples were then incubated at 37˚C for 2.5 hours. To separate the GUVs from aggregates, the samples were subjected to centrifugation using 13000×*g* (here *g* is the acceleration due to gravity) at 20˚C for 20 minutes using a centrifuge machine (NF 800R Centrifuge, Nuve, Turkey). Subsequently, the GUV suspension underwent purification using the membrane filtering method [35]. The purified GUV suspension was transferred to a solution of buffer A containing 0.10 M glucose. The dynamics of the GUVs were observed using a phase contrast microscope (IX 73 Olympus, Japan) with a 20× objective at a temperature of 25 ± 1˚C (Tokai Hit Thermo Plate, Japan). The images of the GUVs were recorded using a charged coupled camera (CCD) (DP22, Olympus) at a speed of 25 frames per second.

2.3 Generating negative membrane potential (φ_{m})

The purified GUVs were transferred to a microchamber of the volume of 200 μL, and the GUVs were diluted using buffer T (10 mM HEPES, 150 mM TEAC, pH 7.5, and 1 mM EGTA) containing 0.10 M glucose. To prevent any effects of osmotic pressure, a similar osmolarity was maintained by keeping the combined concentration of KCl and TEAC inside and outside of the GUVs. Different concentrations of K^+ ions were used to establish a concentration gradient between the inside and outside of the membrane, thereby generating various membrane potentials [20]. In order to prevent strong attachment between the GUVs and the glass surface of the microchamber, a pre-coating step was performed using a 0.10% (w/v) solution of BSA. The membrane potential across the membrane was calculated using the Nernst equation [36]:

$$\varphi_{\mathrm{m}} = 25.7 ln \frac{[\mathrm{K}^+]_{\mathrm{out}}}{[\mathrm{K}^+]_{\mathrm{in}}} \qquad (1)$$

where, $[\mathrm{K}^+]_{\mathrm{out}}$ and $[\mathrm{K}^+]_{\mathrm{in}}$ are the concentrations of K^+ ions outside and inside the GUVs, respectively. The generation of membrane potential is illustrated in Fig 1.

An example to generate $\varphi_{\mathrm{m}} = -30$ mV is given here. The inside $[\mathrm{K}^+]_{\mathrm{in}} = 150$ mM, and hence the final concentration in the outside of GUV is required, $[\mathrm{K}^+]_{\mathrm{out}} = 150\times e^{-25.7/30} =$

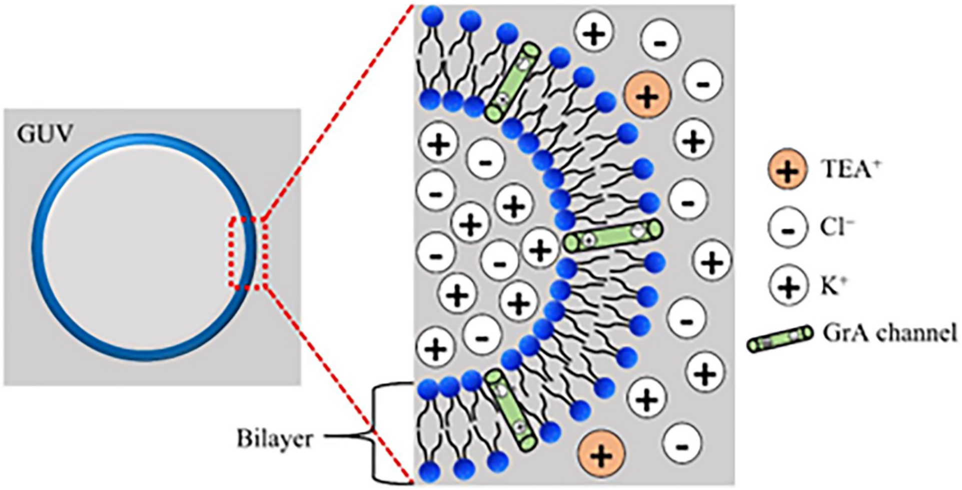

Fig 1. Generating membrane potential across the lipid bilayer. The left side of the figure shows the GUV and the right side shows the concentration of ions across the bilayer.

https://doi.org/10.1371/journal.pone.0291496.g001

46.67 mM. If the final volume of the microchamber was 200 μL, the required purified GUVs is (200 μL×46.67 mM)/150 mM = 62.23 μL, which was diluted with (200 − 62.23) μL = 137.77 μL of buffer T. The same procedure was followed for generating −60 mV and −90 mV. A study successfully demonstrated the establishment of the resulting membrane potential (φ_m) using a specific technique. In the technique, the intensity of the rim of GUV, as indicated by a membrane potential-sensitive dye 3,3'-dihexyloxacarbocyanine iodide DiOC6(3), was employed as a marker of the membrane potential [20]. The study examined the interaction between 2 nM DiOC6(3) and individual DOPG/DOPC/GrA (40/60/0.01)-GUVs in the presence of various membrane potential conditions. We utilized the relevant literature and employed the Nernst equation to calculate the membrane potential in our experiment.

2.4 Electric field-induced membrane tension

After 10 min of transferring GUVs and buffer T into the microchamber, an electric field (E) was applied to the GUVs. When an electric field is applied to GUVs, transmembrane voltage (V_m) is generated across the lipid bilayer. Such voltage leads to induce the lateral electric tension σ_c in the membrane as follows [37]:

$$\sigma_e = \varepsilon_m \varepsilon_0 \left(\frac{h}{2h_e^2}\right) V_m^2 \tag{2}$$

In the equation, ε_m represents the membrane permittivity (~ 4.5), ε_0 is the permittivity of free space, h is the thickness of the membrane (~ 4 nm), and h_e is the membrane dielectric thickness (~ 2.8 nm). When a spherical GUV is exposed to an E, the angle (θ) between the direction of E and the normal to the bilayer surface can range from 0 to 90°. This means that the orientation of E relative to the GUV's membrane can vary throughout the vesicle's surface. The relationship between V_m and θ can be expressed as: $V_m = 1.5RE|\cos\theta|$. The value of V_m is maximum when $\theta = 0°$, corresponding to $V_m = 1.5RE$, which is referred to as the "critical membrane voltage for the breakdown of vesicle" (V_c). By substituting the value of V_m in Eq (2), the following equation can be obtained [38]:

$$\sigma_e = 22.86\ R^2E^2\ (\text{mN/m}) \tag{3}$$

where, R is the radius of the GUVs [m], E is applied electric field [V/m]. Thus, the tension at which a GUV breaks down is influenced by both the applied E and the size of the GUV. If $R = 10$ μm and $E = 553$ V/cm, $V_m = 0.83$ V and $\sigma_e = 7$ mN/m.

2.5 Experimental setup to apply the electric field on the GUVs

We examined the effects of electric field on a 'single GUV' placed in solutions with different membrane potentials (e.g., $\varphi_m = 0, -30, -60$ and -90 mV). The experimental setup for applying the electric field is presented in Fig 2(A). The size of the microchamber and electrode configuration is shown in Fig 2(B). A pulsating DC signal of frequency 1.1 kHz is used in the investigations (Fig 2C). Usually, vesicle suspension contains different sizes of GUVs. We examined a 'single GUV' in each microchamber, in which the size range of GUVs was 30 −35 μm. To obtain statistically reliable results, we repeated the same experiment several times by examining different 'single GUVs' in different microchambers. To apply an electric field to the GUVs, first measured the size of each selected 'single GUV', and then determined the required electric tension using Eq (3). The corresponding range of E was 250–450 V/cm. The electric tension σ_e was applied for a maximum time 60 s. Fig 2(D) shows an illustration of a 'single GUV' between the two gold-coated electrodes. The time when the GUV was completely

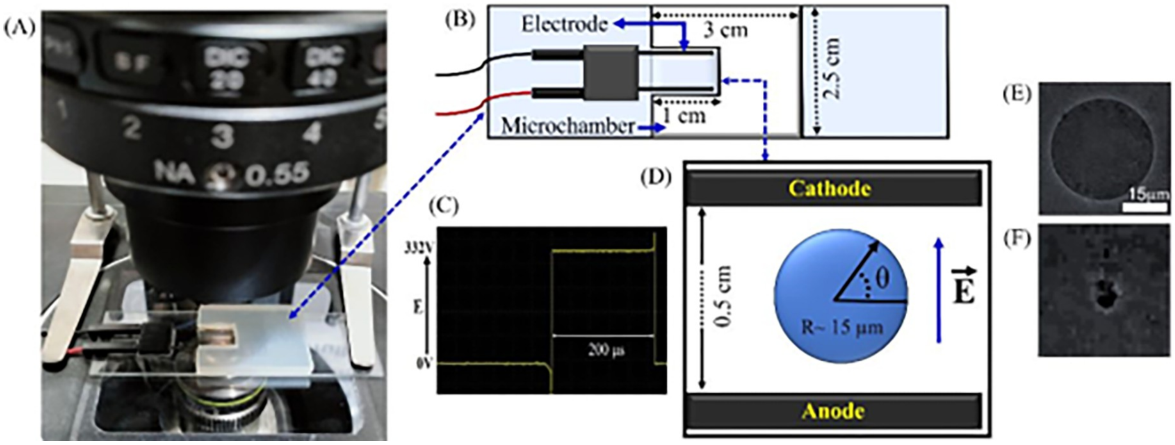

Fig 2. Experimental setup to apply the electric field to the GUVs. (A) Laboratory set up of a microchamber at the stage of a microscope. (B) Schematic representation of the microchamber and gold-coated electrode with proper configuration. The microchamber was fabricated by placing a U-shaped silicone rubber spacer onto a glass slide. (C) Pulsating DC of frequency 1.1 kHz. (D) A 'single GUV' between the gold-coated electrodes, where *E* indicates the electric field. Phase contrast image of (E) intact GUV and (F) ruptured GUV.

https://doi.org/10.1371/journal.pone.0291496.g002

ruptured is defined as the time of pore formation. Before applying the electric field to the GUVs shown in Fig 2(E) and after rupture of the same GUV shown in Fig 2(F).

3. Experimental results

We conducted a comprehensive investigation on the effects of negative membrane potential (φ_m) on the electroporation of lipid vesicles. We varied the membrane potential, electric tension (σ_e), and lipid composition to study their effects. Initially, we explored the electroporation of DOPG/DOPC/GrA (40/60/0.01)-GUVs under different φ_m while maintaining a fixed σ_e. Subsequently, we examined the electroporation of the DOPG/DOPC/GrA (40/60/0.01)-GUVs under various σ_e while keeping the φ_m constant. We calculated the rate constant of rupture (k_r), probability of rupture (P_{rup}), and the average time of intact GUVs (t_{intact}) under these specified conditions. Furthermore, we examined the electroporation of DOPG/DOPC (40/60)-GUVs in HEPES and PIPES buffer. The obtained results were compared with each other for further analysis and insights.

3.1 Electroporation in DOPG/DOPC/GrA (40/60/0.01)-GUVs in the presence of various membrane potentials

At first, we investigated the effects of membrane potential (φ_m) on the electroporation in DOPG/DOPC/GrA (40/60/0.01)-GUVs. Fig 3 shows the experimental results of the rupture of GUVs at 0 and −90 mV at $\sigma_e = 6$ mN/m. Without applying electric field (i.e., 0 s), the GUVs become intact and spherical in shape, as shown in Fig 3(A) and 3(B). At $\varphi_m = 0$, the GUV remains intact until 40.62 s (Fig 3A). GUV starts to rupture at 42.99 s, and at 43.2 s, it becomes completely ruptured as the structure of the GUV disappears. Similarly, at $\varphi_m = -90$ mV, GUV is started to rupture at 18.26 s (Fig 3B). The rupture occurs due to the rapid increase in the radius of the pores formed in the GUV membranes. The starting time of rupture indicates the time of pore formation, signifying the point at which the structural integrity of the GUV disappears.

The same experiments were carried out for several 'single GUVs' (number of examined GUVs was $N = 12–18$) in each independent experiment (number of independent experiments was $n = 2–4$) under the same conditions. The rupture time (t_{rup}) for several GUVs in one

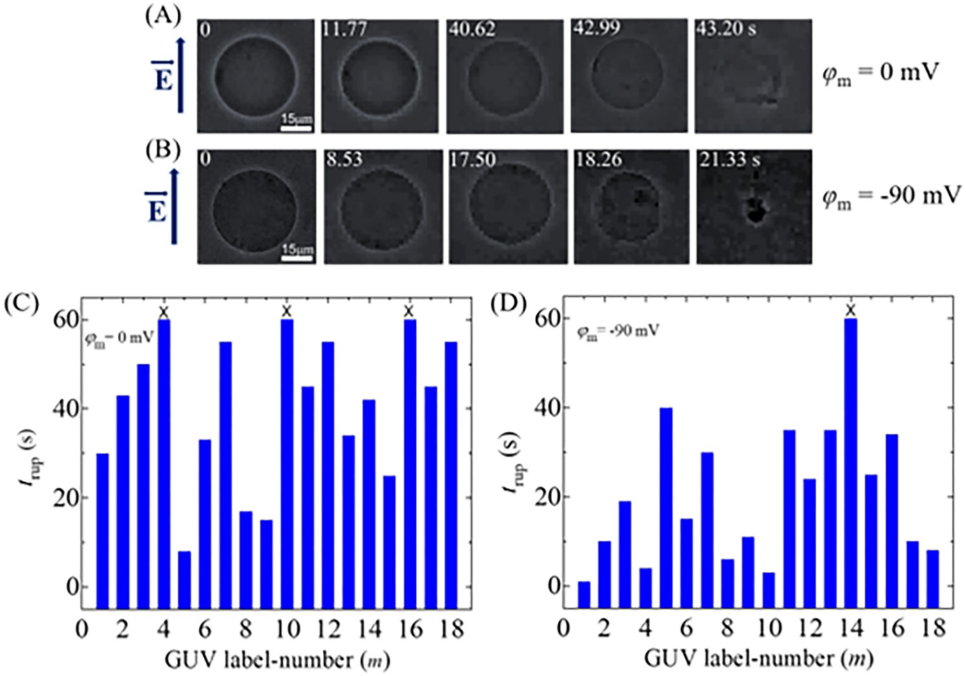

Fig 3. Rupture of DOPG/DOPC/GrA (40/60/0.01)-GUVs for 0 and −90 mV at σ_e = 6 mN/m. Phase contrast images of rupture of a 'single DOPG/DOPC/GrA (40/60/0.01)-GUV' at (A) φ_m = 0, and (B) φ_m = −90 mV. The electric field (*E*) direction is shown with an arrow on the left side. The numbers in each image show the time in seconds after applying *E*. The stochastic rupture of several 'single GUVs' at (C) φ_m = 0, and (D) φ_m = −90 mV.

https://doi.org/10.1371/journal.pone.0291496.g003

independent experiment is different both for 0 mV and −90 mV, indicating the stochastic nature of rupture (Fig 3C and 3D). The required rupture time of several GUVs at 0 mV is relatively larger compared to −90 mV. In Fig 3(C), 15 GUVs rupture out of 18 GUVs at 0 mV, whereas 17 GUVs rupture at −90 mV (Fig 3D). The time required to rupture the GUVs is defined as the rupture time of vesicles ($t_{\rm rup}$). A 'single GUV' was observed until 60 s, whether the GUV ruptured or not. If any GUVs didn't rupture within 60 s, they are considered intact and indicated by a symbol (×) mark at the top of the bar (Fig 3C and 3D). A similar rupture along with stochastic rupture of DOPG/DOPC/GrA (40/60/0.01)-GUVs is also observed for −30 mV and −60 mV at σ_e = 6 mN/m.

To determine the rate constant of rupture of GUV (k_r) for different negative membrane potentials at a fixed σ_e, the time course of the fraction of intact GUVs without rupture among all the examined GUVs, $P_{\rm intact}$ (t), is determined, which indicates on how much fraction of GUVs became intact with time and is represented as $P_{\rm intact}$ (t) = 1- $P_{\rm rup}$ (t). If 18 single GUVs are examined at σ_e = 6 mN/m in which 9 GUVs rupture within 60 s observation, $P_{\rm intact}$ (t) = 1- $P_{\rm pore}$ (t) = 1–9/18 = 0.5. Fig 4(A) shows the time course of $P_{\rm intact}$ (t) for different membrane potentials at 6 mN/m. It shows that the decrement of experimental data for $P_{\rm intact}$ (t) vs. time is a factor when membrane potential changes from 0 to −90 mV. The $P_{\rm intact}$ (t) vs. time graph is well fitted by a single-exponential decay function,

$$P_{\rm intact}(t) = \exp(-k_r t) \tag{4}$$

where, t is the duration of time to apply the tension in GUVs. From the fitted curves, the values of k_r are obtained 6.2×10^{-3}, 10.4×10^{-3}, 21.8×10^{-3}, and 36.7×10^{-3} s^{-1} for 0, −30, −60 and −90 mV, respectively. The same experiments were carried out for several 'single GUVs' (N = 12 −18) in each independent experiment (n = 2–4). The values of average k_r are (7.5 ± 1.6)×10^{-3},

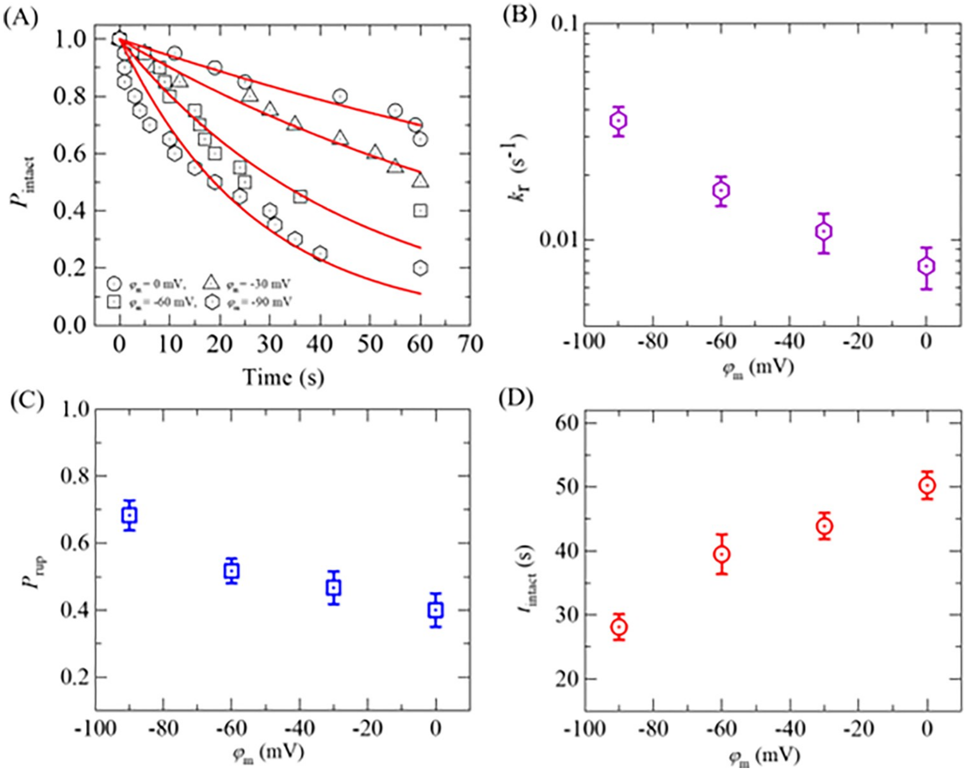

Fig 4. Rate constant of rupture, probability of rupture, and the average time of intact DOPG/DOPC/GrA (40/60/0.01)-GUVs in the presence of various φ_m at 6 mN/m. (A) Time course of P_{intact} for 0, −30, −60, and −90 mV. The membrane potential dependent (B) rate constant, (C) probability, and (D) average time of intact GUVs.

https://doi.org/10.1371/journal.pone.0291496.g004

$(10.9 \pm 2.3)\times10^{-3}$, $(16.9 \pm 2.6)\times10^{-3}$, and $(35.6 \pm 5.5)\times10^{-3}$ s^{-1} for 0, −30, −60 and −90 mV, respectively, at 6 mN/m. Hence, the values of k_r increase with the increase of negative membrane potential (Fig 4B).

We have calculated the probability of rupture (P_{rup}) and the average time of intact (t_{intact}) of DOPG/DOPC/GrA (40/60/0.01)-GUVs for different φ_m at 6 mN/m. The values of P_{rup} were 0.41 ± 0.05, 0.47 ± 0.02, 0.52 ± 0.02, and 0.68 ± 0.04 for 0, −30, −60, and −90 mV, respectively (Fig 4C). P_{rup} increases with the increase of φ_m. The average times of intact GUVs (t_{intact}) are 50.25 ± 2.1, 43.88 ± 2.0, 39.50 ± 3.1, and 28.11 ± 2.0 s for 0, −30, −60, and −90 mV, respectively, at 6 mN/m. Less intact time of GUVs is observed in higher φ_m (Fig 4D).

Now, we quantify the change in rate constant of rupture, probability of rupture, and the average time of intact DOPG/DOPC/GrA(40/60/0.01)-GUVs at $\sigma_e = 6$ mN/m with the change in membrane potential. Table SI 1 in S1 File represents the values of different parameters in the presence of φ_m. Table SI 2 in S1 File is extracted from Table SI 1 in S1 File, which presents the changes in k_r, P_{rup}, and t_{intact} due to the changes in φ_m. The average values of $\Delta k_r/\Delta\varphi_m$, $\Delta P_{\text{rup}}/\Delta\varphi_m$, and $|\Delta t_{\text{intact}}|/\Delta\varphi_m$ are obtained 1.1×10^{-4} (s^{-1}/mV), 2.3 (mV^{-1}), and 22.3×10^{-2} (s/mV), respectively, at $\sigma_e = 6$ mN/m and at $\varphi_m = -30$ mV.

3.2 Electroporation in DOPG/DOPC/GrA (40/60/0.01)-GUVs in the presence of various electric tensions at $\varphi_m = -30$ mV

In this section, we have investigated the electric tension (σ_e) dependent electroporation in DOPG/DOPC/GrA (40/60/0.01)-GUVs at $\varphi_m = -30$ mV, and presented the results in Fig 5.

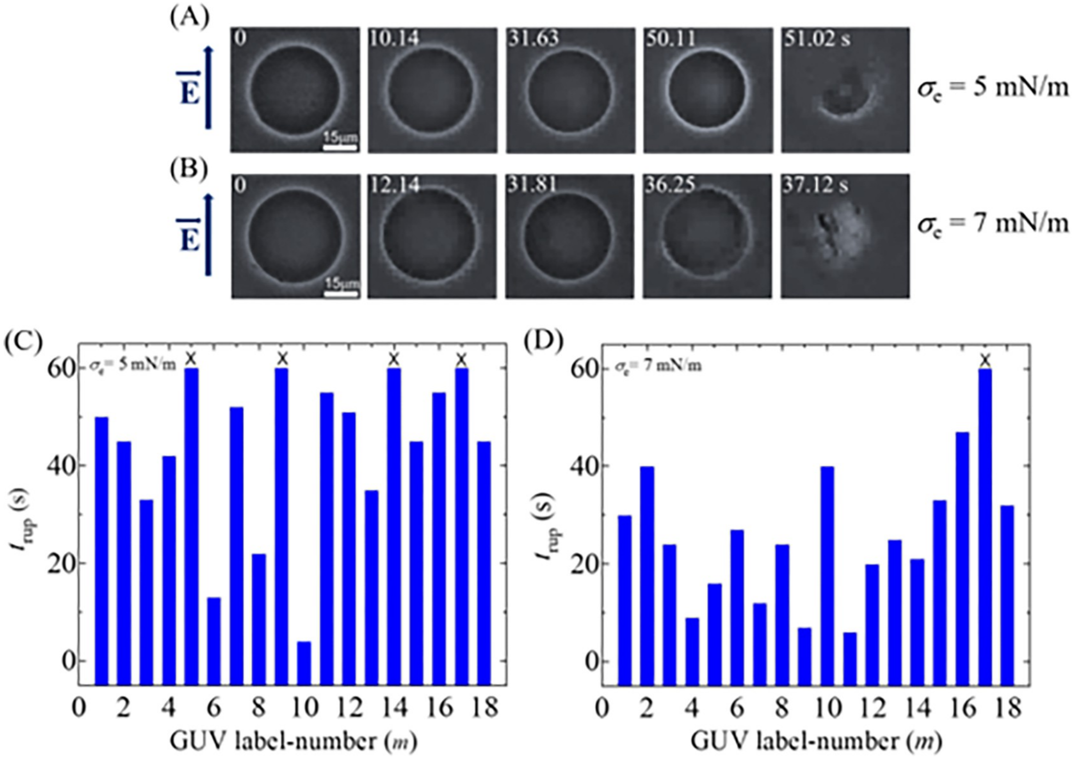

Fig 5. Rupture of DOPG/DOPC/GrA (40/60/0.01)-GUVs at 5 and 7 mN/m in the presence of −30 mV. Phase contrast images of rupture of a 'single DOPG/DOPC/GrA (40/60/0.01)-GUV' at (A) σ_e = 5 mN/m and (B) σ_e = 7 mN/m. The electric field (*E*) direction is shown with an arrow on the left side. The numbers in each image show the time in seconds after applying *E*. The stochastic rupture of several 'single GUVs' at (C) σ_e = 5 mN/m, and (D) σ_e = 7 mN/m.

https://doi.org/10.1371/journal.pone.0291496.g005

The phase contrast images of two separate 'single GUVs' at 5 and 7 mN/m are presented in Fig 5(A) and 5(B), respectively in the presence of φ_m = -30 mV. Both the GUVs remain intact and spherical before applying the electric filed (i.e., 0 s). The complete rupture of these GUVs occurs at 51.02 and 37.12 s at 5 and 7 mN/m, respectively. The stochastic rupture of several 'single GUVs' for both conditions is shown in Fig 5C and 5D. The unruptured GUVs are indicated by (×) mark at the top of the respective bar diagram. The number of ruptured GUVs at 5 mN/m is relatively smaller compared to 7 mN/m.

Now, we determine the values of k_r of DOPG/DOPC/GrA (40/60/0.01)-GUVs under various σ_e. We follow the same procedure as in Section 3.1 for determining the k_r. The experimental data on the time course of P_{intact} for various σ_e are presented in Fig 6(A). The experimental data for each tension is fitted using Eq (4), and the values of k_r are obtained as 7.1×10^{-3}, 10.4×10^{-3}, and 17.9×10^{-3} s^{-1} for 5, 6 and 7 mN/m, respectively. The average values of k_r (N = 18–20, n = 2–4) are obtained as $(7.1 \pm 1.3)\times10^{-3}$, $(10.4 \pm 1.5)\times10^{-3}$, and $(17.9 \pm 4.3)\times10^{-3}$ s^{-1} for 5, 6, and 7 mN/m, respectively, at −30 mV. It shows the increasing of k_r with the increase of σ_e at −30 mV (Fig 6B). Now, we compare these rate constants with those obtained at 0, −60, and −90 mV. At 5 mN/m, the k_r values are $(4.1 \pm 1.2)\times10^{-3}$, $(7.1 \pm 1.3)\times10^{-3}$, and $(20.1 \pm 5.8)\times10^{-3}$ s^{-1} for 0, −30, and −90 mV, respectively. The similar differences in k_r for different φ_m are also observed at 6 and 7 mN/m (Fig 6B). Thus, at a fixed tension σ_e, φ_m greatly increases the kinetics of vesicle rupture. We have calculated the probability of rupture (P_{rup}) for various φ_m and σ_e. At σ_e = 6 mN/m, the values of P_{rup} are found as 0.35 ± 0.05, 0.47 ± 0.07, and 0.68 ± 0.07 for 0, −30, and −90 mV, respectively. The same trend of increasing the values of P_{rup} with φ_m is obtained for 5 and 7 mN/m. The σ_e

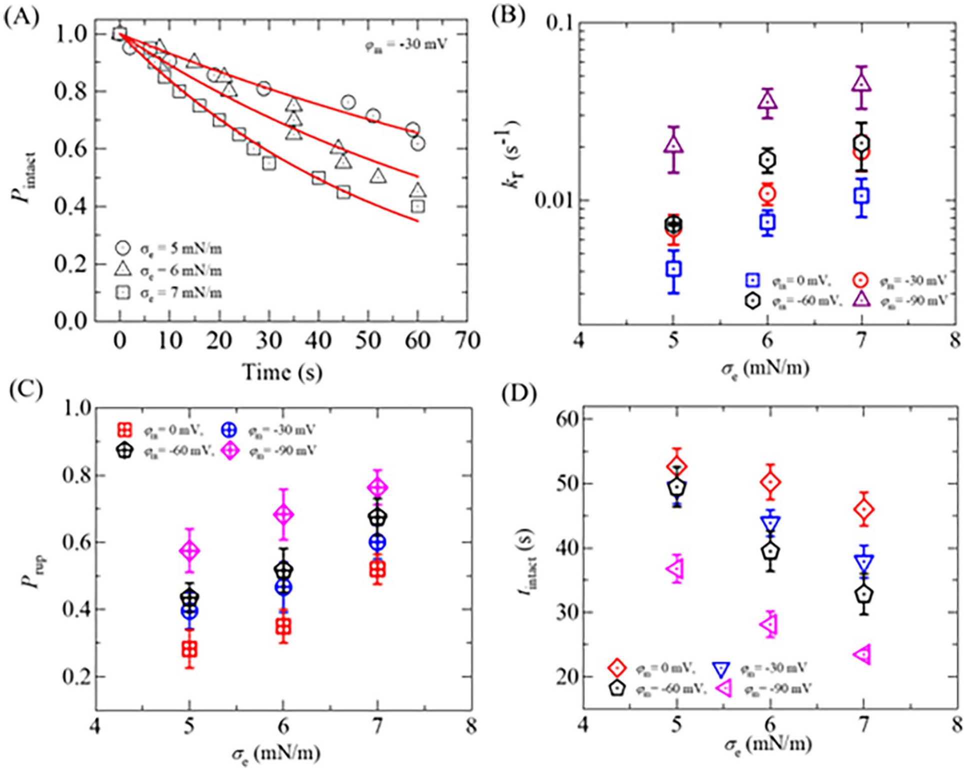

Fig 6. Rate constant of rupture, probability of rupture, and the average time of intact DOPG/DOPC/GrA (40/60/0.01)-GUVs in the presence of various φ_m and σ_e. (A) Time course of P_{intact} for 5, 6, and 7 mN/m at $\varphi_m = -30$ mV. The σ_e dependent (B) rate constant, (C) probability, and (D) average time of intact GUVs for different φ_m.

https://doi.org/10.1371/journal.pone.0291496.g006

dependent P_{rup} for various φ_m is presented in Fig 6(C), indicating that the presence of higher φ_m increases the probability of rupture of GUVs irrespective of membrane tension. In a similar way, the values of the average time of intact (t_{intact}) are obtained as 37.4 ± 4.8, 29.7 ± 2.8, and 19.8 ± 2.7 s for 5, 6, and 7 mN/m, respectively, at −30 mV. At 0 mV, the values of t_{intact} are obtained 41.4 ± 2.8, 35.4 ± 2.7, and 29.2 ± 2.4 s for 5, 6, and 7 mN/m, respectively. Similarly, at −90 mV, these values are obtained as 19.6 ± 2.7, 14.5 ± 3.0, and 13.7 ± 2.2 s for the corresponding tensions. It is observed that less time is required for vesicle rupture at higher φ_m at a particular tension (Fig 6D).

3.3 Estimation of pore edge tension (Γ) of DOPG/DOPC (40/60)-GUVs under various conditions

Lipid membranes, composed of lipid molecules, exhibit continuous fluctuations in their lateral density. These fluctuations can lead to localized regions of decreased lipid density known as prepores or local density rarefactions [39,40]. The presence of an electric field (E) induces lateral tension (σ_e) in the membranes. Thermal energy further contributes to variations in the lateral density of lipid molecules, causing local condensation and rarefaction within the membrane [38]. When a rarefaction in the membrane exceeds a critical radius, r_c, it transitions into a prepore with a radius, r. If r is smaller than r_c, the prepore closes rapidly. Conversely, if r is greater than or equal to r_c, the prepore transforms into a transmembrane pore. These phenomena are depicted and visualized in Fig 7. Vesicle rupture occurs within a very short time, approximately 1 s, as the radius, r, approaches infinity. The free energy of a prepore, $U(r, \sigma_e)$,

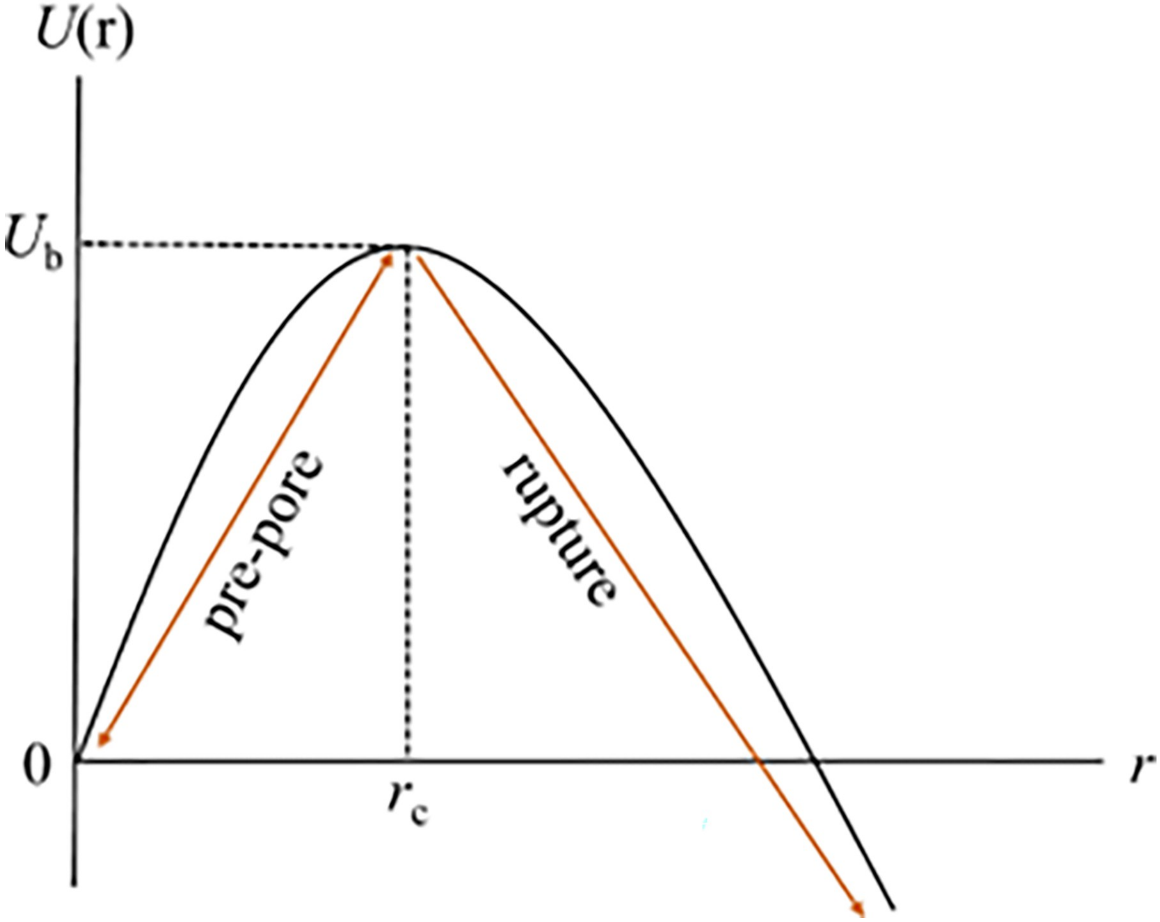

Fig 7. Prepore energy profile. The energy landscape consists of prepore region and the rupture region.

https://doi.org/10.1371/journal.pone.0291496.g007

comprises a term -$\pi r^2\sigma_e$ that favor prepore expansion and the term $2\pi r\Gamma$ that favor prepore closure, where Γ represents the free energy per unit length of a prepore (i.e., pore edge tension or line tension of a pore). According to the classical theory of pore formation, the free energy of a prepore can be expressed as [41]:

$$U(r,\ \sigma_e) = 2\pi r\Gamma - \pi(\sigma_e + B)r^2 \tag{5}$$

In our previous paper [42], a similar equation for the free energy of a prepore in the context of IRE was utilized. In that study, we specifically considered the toroidal structure of the prepore [43]. The parameter B represents the electrostatic interaction arising from the surface charge of membrane. In our case, B is considered to be 1.76 mN/m since the surface charge density of the DOPG/DOPC/GrA (40/60/0.01)-GUVs and the ion concentration in the buffer match those of DOPG/DOPC (40/60)-GUVs [41]. The energy barrier, or activation energy, for pore formation is determined by the maximum value of $U(r)$ at $r = r_c$, denoted as U_b. At $r_c = \Gamma/\ (\sigma_e + B)$, U_b, is expressed as follows [44,45]:

$$U_b = \frac{\pi\Gamma^2}{(\sigma_e + B)} \tag{6}$$

The Arrhenius equation for the rate constant (k_r) can be derived from Eq (6) and can be expressed as follows [46]:

$$k_r = A \exp\left[-\frac{\frac{\pi\Gamma^2}{(\sigma_e+B)}}{k_B T}\right] \tag{7}$$

where, A is the frequency factor, k_B is the Boltzmann constant, and T is the absolute temperature. By rearranging Eq (7), we can derive the revised expression as follows:

$$\ln k_r = \ln \mathrm{A} - \frac{\pi\Gamma^2}{k_B T}\left(\frac{1}{(\sigma_e + B)}\right) = \mathrm{C} - \frac{\pi\Gamma^2}{k_B T}\left(\frac{1}{(\sigma_e + B)}\right) \tag{8}$$

The experimental data on lnk_r vs. $1/(\sigma_e + B)$ for several membrane potentials are fitted using Eq (8) as shown in Fig 8. The best-fit values were obtained for $\Gamma = 4.80 \pm 1.98$, 6.14 ± 2.23, 6.47 ± 3.18, and 5.48 ± 2.12 pN at 0, −30, −60, and −90 mV respectively. The change in Γ is negligible and often unchanged with respect to the change of φ_m. Therefore, it can be assumed that the value of Γ is almost same for DOPG/DOPC/GrA (40/60/0.01)-GUVs with the change in φ_m.

3.4 Electroporation in DOPG/DOPC (40/60)-GUVs in HEPES and PIPES buffer in the absence of membrane potential

In this experiment, the electric field-induced rupture of DOPG/DOPC (40/60)-GUVs prepared in HEPES buffer (10 mM HEPES, 150 mM KCl, pH 7.5, and 1 mM EGTA) is

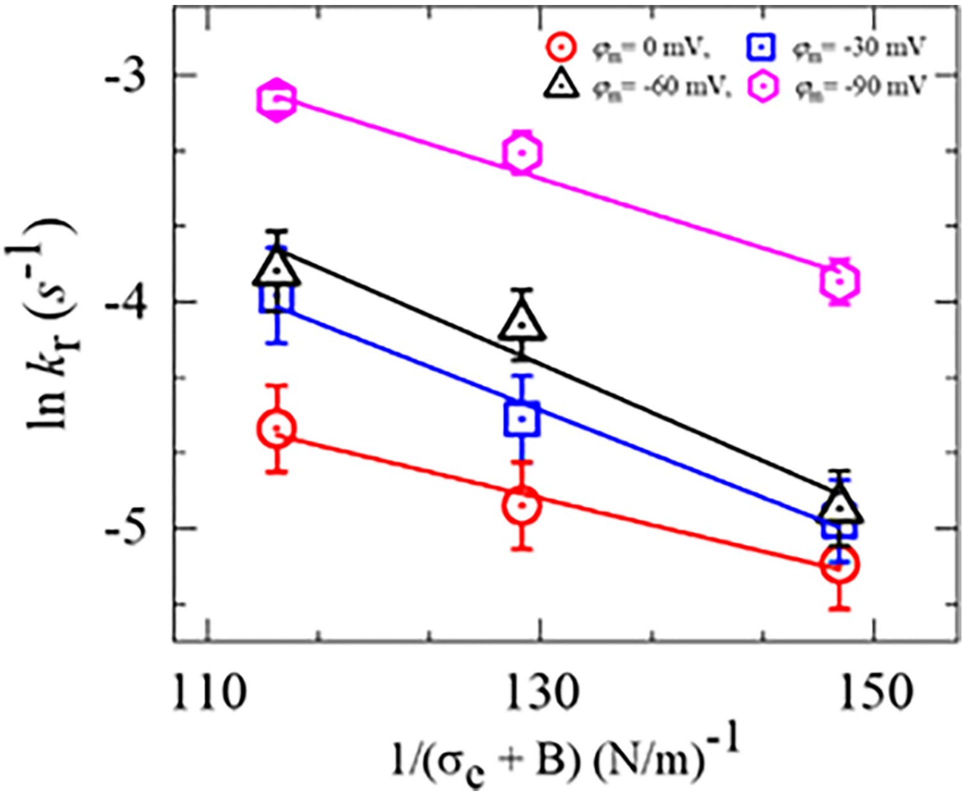

Fig 8. The $1/(\sigma_e + B)$ dependent lnk_r of DOPG/DOPC/GrA (40/60/0.01)-GUVs in the presence of various φ_m. The solid line is the best-fit theoretical curve of Eq (8).

https://doi.org/10.1371/journal.pone.0291496.g008

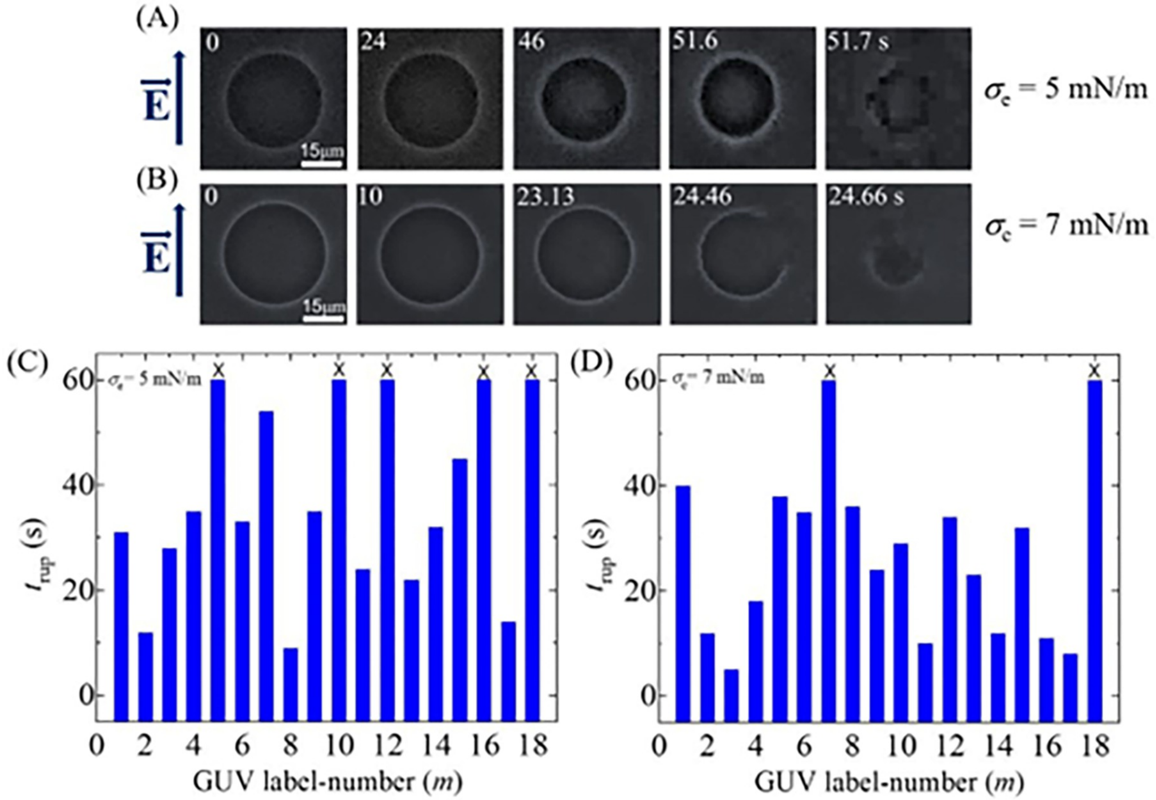

Fig 9. Rupture of DOPG/DOPC (40/60)-GUVs in HEPES buffer. Phase contrast images of rupture of a 'single DOPG/DOPC (40/60)-GUV' at (A) σ_e = 5 mN/m, and (B) σ_e = 7 mN/m. The electric field (E) direction is shown with an arrow in the left side. The numbers in each image show the time in seconds after applying E. The stochastic rupture of several 'single GUVs' at (C) σ_e = 5 mN/m, and (D) σ_e = 7 mN/m.

https://doi.org/10.1371/journal.pone.0291496.g009

investigated in the absence of membrane potential. Fig 9 shows the experimental results of GUV's rupture under different tensions. Initially, at 0 s, both GUVs (shown in Fig 9(A) and 9 (B)) remain intact and exhibit a spherical shape with high contrast in the phase contrast image, indicating their stability. However, when an electric tension of σ_e = 5 mN/m is applied to the GUV shown in Fig 9(A), rupture occurs at 51.6 s. Similarly, when a higher electric tension of σ_e = 7 mN/m is applied to the GUV shown in Fig 9(B), rupture occurs at 24.46 s. The stochastic rupture of several GUVs at σ_e = 5 mN/m and σ_e = 7 mN/m is presented in Fig 9C and 9D, in which the horizontal axis indicates the GUV label number (m) and the vertical axis indicates the rupture time (t_{rup}). The GUVs that did not rupture within this time frame is indicated by the cross (×) mark on top of the bar (Fig 9C and 9D).

To determine the k_r of DOPG/DOPC (40/60)-GUVs, the time-dependent P_{intact} is shown in Fig 10(A). The P_{intact} vs. time graph is fitted using Eq 4, and the k_r value is obtained 5.8×10^{-3} s^{-1} for 5 mN/m. Similarly, the values of k_r are 10.4×10^{-3} s^{-1} and 15.1×10^{-3} s^{-1} for 6 and 7 mN/m, respectively. The average values of k_r with (± SE) from the several independent experiments (e.g., N = 12–18, n = 2–4) are obtained $(4.8 \pm 1.6)\times10^{-3}$ s^{-1}, $(9.1 \pm 3.2)\times10^{-3}$ s^{-1} and $(16 \pm 5.4)\times10^{-3}$ s^{-1} for 5, 6, and 7 mN/m, respectively (Fig 10B). This is clearly indicating the increasing rate constant with applied field. The values of P_{rup} are obtained 0.36 ± 0.05, 0.45 ± 0.06, and 0.54 ± 0.06 for 5, 6, and 7 mN/m, respectively (Fig 10C). It is found that the P_{rup} increases with the increase in applied tension. As mentioned above, all the examined GUVs were not ruptured in some cases. The average time of intact (t_{intact}) GUVs were

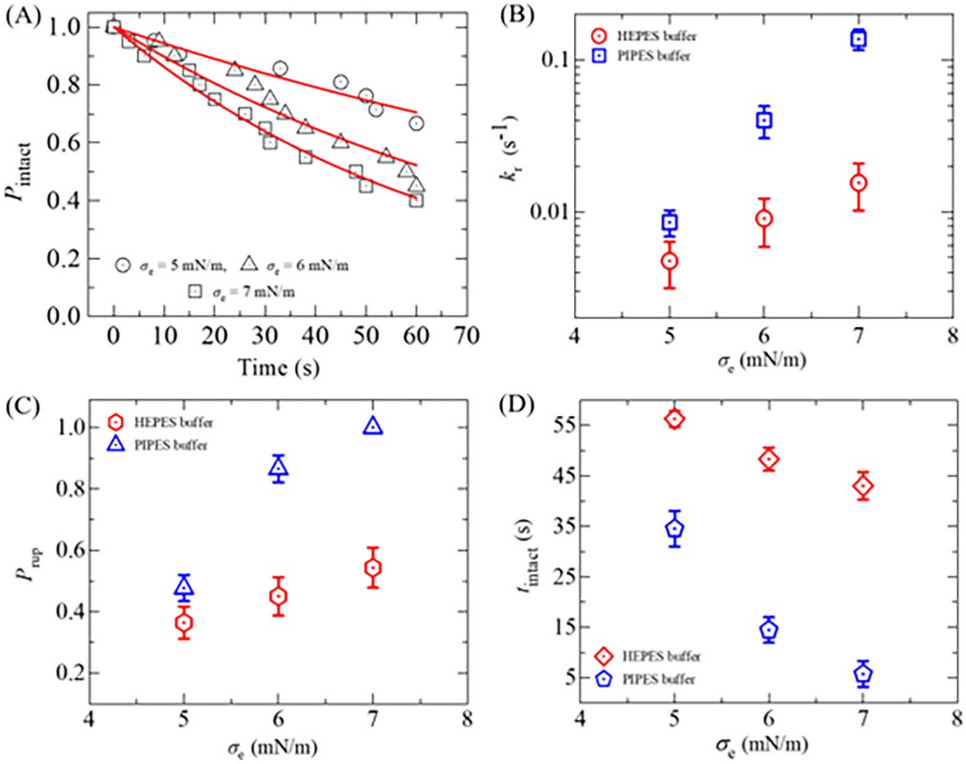

Fig 10. Rate constant of rupture, probability of rupture, and the average time of intact DOPG/DOPC (40/60)-GUVs prepared in HEPES buffer. (A) Time course of P_{intact} for various σ_e. The σ_e dependent (B) rate constant, (C) probability, and (D) average time of intact GUVs.

https://doi.org/10.1371/journal.pone.0291496.g010

56.32 ± 1.6, 48.33 ± 2.3, and 43.03 ± 2.8 s for 5, 6, and 7 mN/m, respectively (Fig 10D). The intact time is comparatively shorter at higher membrane tensions.

We also performed the similar experiments in PIPES buffer (10 mM PIPES, 150 mM NaCl, pH 7.5, and 1 mM EGTA) and the results follow the same trend as those obtained in HEPES buffer (Fig 11). The values of k_r, P_{rup} and t_{intact} at σ_e = 5 mN/m in PIPES buffer are obtained $(8.5 \pm 1.7)\times10^{-3}$ s^{-1}, 0.36 ± 0.05, and 34.5 ± 3.5 s, respectively, whereas the corresponding values in HEPES buffer are obtained $(4.8 \pm 1.6)\times10^{-3}$ s^{-1}, 0.48 ± 0.04, and 56.3 ± 1.8 s. These differences are due to the presence of different salts and other chemicals in the two buffers. The experimental data on lnk_r vs. $1/(\sigma_e + B)$ is presented in Fig 11, and the data points have been fitted using Eq (8). The best-fit values of Γ are obtained as Γ = 10.4 ± 0.9 pN for PIPES buffer and Γ = 6.8 ± 1.3 pN for HEPES buffer. Hence, the Γ for DOPG/DOPC (40/60)-GUVs in PIPES buffer is 1.5 times larger than that of HEPES buffer. The value of Γ for DOPG/DOPC (40/60)-GUVs in the PIPES buffer is very similar to that obtained in the literature [31].

4. Discussion

We examined the electroporation of DOPG/DOPC/GrA (40/60/0.01)-GUVs at different negative membrane potentials (φ_m) while keeping electric tension (σ_e) constant (Figs 3 and 4). We also investigated the electroporation of DOPG/DOPC/GrA (40/60/0.01)-GUVs at a fixed φ_m by varying σ_e (Figs 5 and 6). In both cases, we observed an increase in both rate constant of rupture (k_r) and probability of rupture (P_{rup}) with increasing φ_m. Moreover, the time required for GUV rupture decreased as φ_m increased. The application of σ_e also resulted in an enhancement of electroporation kinetics. The estimated pore edge tension (Γ) is almost similar under

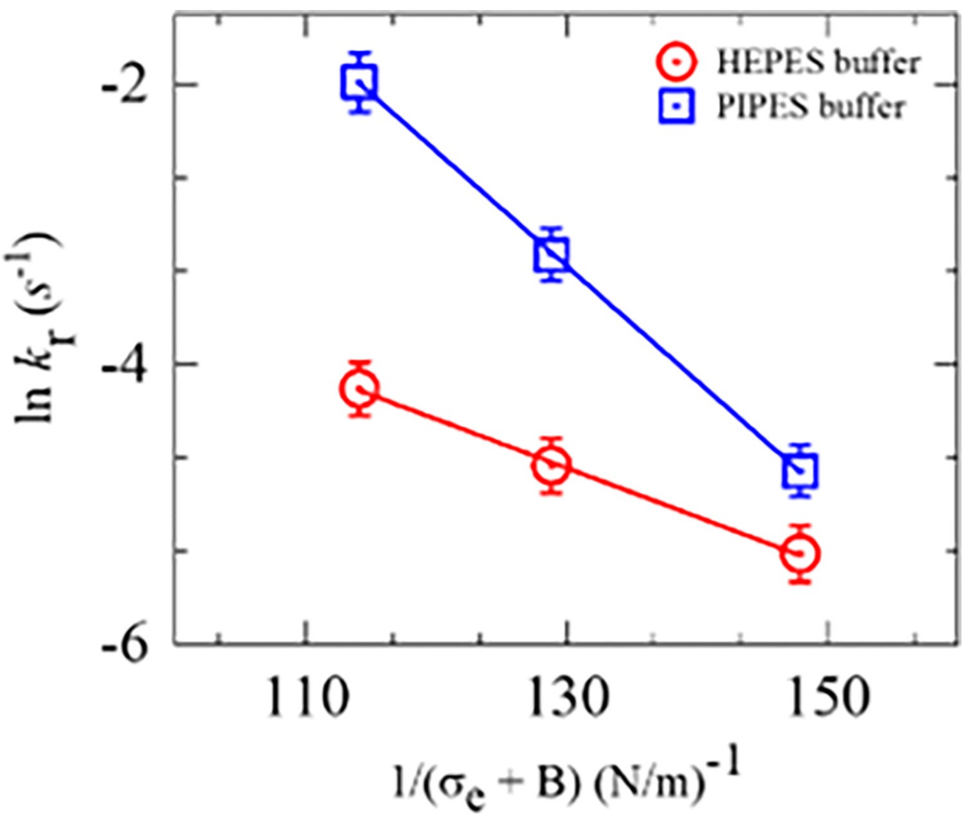

Fig 11. The 1/(σ_e +B) dependent lnk_r of DOPG/DOPC (40/60)-GUVs obtained for HEPES and PIPES buffer. The solid line is the best-fit theoretical curve of Eq (8).

https://doi.org/10.1371/journal.pone.0291496.g011

various φ_m (Fig 8). Basically, Γ is an intrinsic membrane property originating from the physicochemical properties and the amphiphilic nature of lipid molecules in the membranes [27]. Since, the concentration of ions (whether K^+ or a combination of K^+ and TEAC+) in the inside and outside of GUVs remain the same for different φ_m, Γ is expected to be the same for different φ_m, which agrees with our estimation of Γ.

To elucidate the kinetics of electroporation in the presence of φ_m, it is necessary to consider how the membrane potential induces lateral stretching in the membranes. One model predicts that the application of a potential can led to thinning of the membranes, resulting in changes in the membrane thickness (h) [47]. The thinning of the membrane in response to φ_m can be attributed to changes in the capacitance of the bilayer membrane. The change in capacitance can be expressed as $\Delta C = C_m (X_T + 2X_E)$, where C_m represents the capacitance, and X_T and X_E are the fractional increases in area due to bilayer formation and elastic stress, respectively. In the case of an incompressible membrane, a decrease in membrane thickness occurs in proportion to the increase in membrane area caused by elastic stretching. The parameter X_E, which represents the fractional increase in area due to elastic stress, is inversely proportional to the membrane elasticity. Therefore, a more elastic membrane will exhibit a smaller value of X_E. If a change in φ_m leads to an overall decrease in membrane thickness (h) before rupture, it is expected that the rupture will be directly preceded by a change in the C_m. This change in capacitance indicates a change in the effective area of the membrane, reflecting the thinning process. It is worth noting that the membrane volume remains essentially unchanged during this process since the volume compressibility of the membrane material is nearly constant.

Therefore, the decrease in thickness is accompanied by an increase in area, while the overall volume of the membrane remains relatively constant [48,49]. Based on these researches, we have considered the additive nature of tension, such as the total membrane tension $\sigma_t = \sigma_e + \sigma_\varphi$, where, σ_φ is induced due to the presence of φ_m. The value of σ_φ depends on the magnitude of the φ_m. Specifically, as the membrane potential increases, the corresponding tension induced by the membrane potential, σ_φ, becomes larger. In the absence of φ_m, $\sigma_t = \sigma_e$ as $\sigma_\varphi = 0$.

The additive nature of tensions has been considered in several investigations, as discussed in the following studies. It has been well-reported that the presence of osmotic pressure increases the rupture of vesicles due to both mechanical tension (σ_m) [50] and electric tension (σ_e) [51]. These studies have explained that osmotic pressure adds an additional tension, denoted as σ_{os}, to the externally applied σ_m or σ_e. Therefore, the total tension experienced by the membranes of GUVs during electroporation can be expressed as $\sigma_t = \sigma_e + \sigma_{os}$. Similarly, during mechanical tension in the presence of osmotic pressure, the total tension can be expressed as $\sigma_t = \sigma_m + \sigma_{os}$. It should be noted that the tension generated due to osmotic pressure depends on the concentration gradient between the inner and outer regions of the GUVs. In another recent investigation on magainin 2-induced pore formation in lipid vesicles, the additive nature of tensions was also observed. In this case, a 'single GUV' was held at the tip of a micropipette, and a magainin 2 solution was introduced in the vicinity of the GUVs through another micropipette [52–54]. The total tension experienced by the membrane in this scenario can be expressed as $\sigma_t = \sigma_{mag} + \sigma_m$, where σ_{mag} is induced due to the surface concentration of magainin 2.

We investigated how the energy barrier of a prepore changes with the φ_m. In our analysis, as for simplicity, we considered a constant value of $\Gamma = 6.0$ pN for all cases of φ_m, and a fixed value of $\sigma_e = 6$ mN/m to calculate the k_r. The relationship between the energy barrier and the induced tension due to applying membrane potential across the membrane was described using Eq (7), where the parameter A was considered 13500 s^{-1}. The simulated data, presented in Table 1, exhibits a strong correlation with the experimental data. This supports our proposal regarding the additive nature of σ_φ with σ_e, which provides a reasonable explanation for the observed increasing trend in electroporation events (e.g., the rate constant of rupture and probability of rupture) of GUVs in the presence of φ_m (as shown in Figs 4 and 6).

The energy barrier of a prepore decreases with an increase of negative membrane potential, as depicted in Fig 12. The calculated barrier energy ranged from 14.41 to 12.84 k_BT as φ_m increased from 0 to −90 mV. Notably, these barrier energy values closely align with those obtained in electroporation and micropipette aspiration techniques [13].

The rim of a pore may be formed by the connection of the outer and inner monolayers in a toroidal fashion, as illustrated in Fig 13 [43,55]. This toroidal pore structure represents a characteristic feature of the membrane during the process of pore formation.

The primary objective of utilizing GrA was to create ion channels across the lipid bilayer. These ion channels play a pivotal role in establishing a membrane potential across the lipid

Table 1. A comparison of rate constant between estimated and experimental data for various membrane potentials.

Membrane potential φ_m (mV)	Membrane tension due to φ_m σ_φ (mN/m)	Rate constant k_r (s^{-1}) [Using Eq 7]	Rate constant k_r (s^{-1}) [Expt. of Fig 8B]
0	0	7.5×10^{-3}	$(7.5 \pm 1.6)\times10^{-3}$
−30	0.210	10.9×10^{-3}	$(10.9 \pm 2.3)\times10^{-3}$
−60	0.465	16.9×10^{-3}	$(16.9 \pm 2.6)\times10^{-3}$
−90	0.943	35.5×10^{-3}	$(35.6 \pm 5.5)\times10^{-3}$

https://doi.org/10.1371/journal.pone.0291496.t001

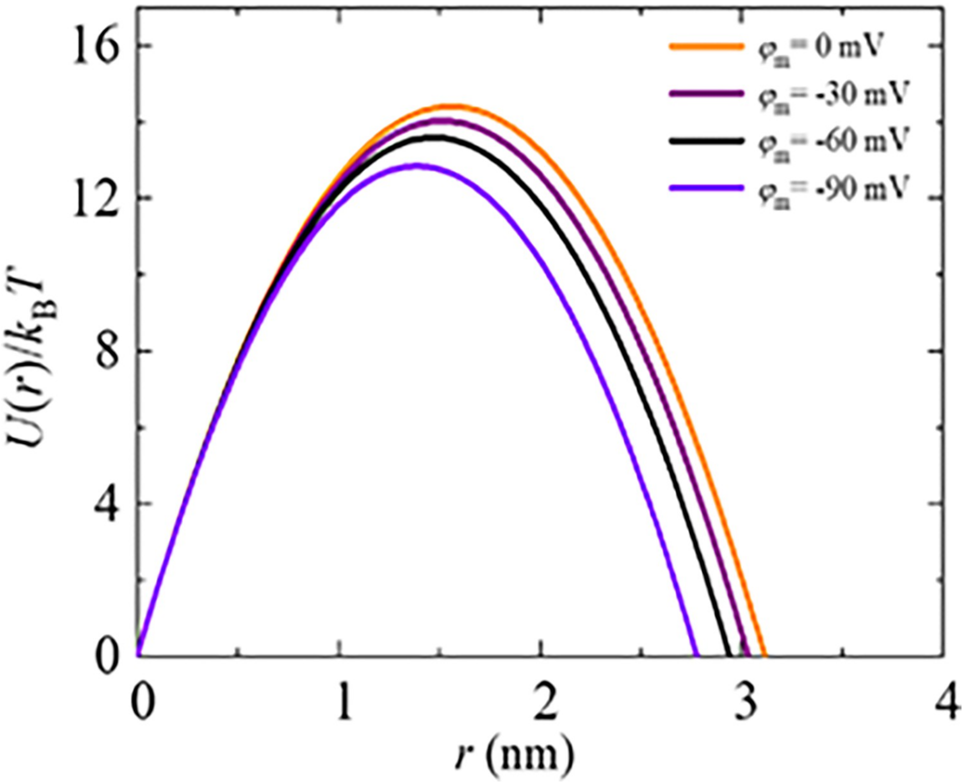

Fig 12. The prepore energy profile in the presence of various membrane potentials. The energy barrier is calculated using Eq (5).

https://doi.org/10.1371/journal.pone.0291496.g012

membrane. It is well-documented that introducing GrA into the membrane significantly impacts the surface tension of the membranes [56]. Furthermore, GrA has a notable influence on the spontaneous curvature of the monolayer of DOPC lipid [57]. Consequently, the presence of GrA brings about changes in the mechanical properties and the spontaneous curvature of the monolayer. These alterations have a direct effect on the electroporation kinetics of DOPG/DOPC/GrA (40/60/0.01)-GUVs, leading to modified behavior in these lipid vesicles.

Numerous studies have reported that membrane potential plays a crucial role in various cellular processes, including T-cell signaling [58], antimicrobial peptide-induced pore formation, and the entry of cell penetrating peptide [32]. It has been observed that an increase in the binding constant between peptides and membranes is a key factor in enhancing poration kinetics [21]. Consequently, it has become evident from this study that the presence of φ_m facilitates increased poration and poration kinetics in lipid vesicles. This observation further supports our investigation, indicating that electroporation in GUVs is enhanced by φ_m (Figs 4 and 6).

In our study, we used KCl and TEAC salts with a combined concentration of 150 mM, similar to the previously used NaCl salt [41]. These salts are also monovalent, and their concentration was maintained at 150 mM. The lipid composition of our study remains consistent with our previously published papers, consisting of DOPG/DOPC (40/60)-GUVs [41]. Therefore, parameter B is considered unchanged throughout the estimation Γ. For the sake of simplicity, we did not include the term U_0 in the pre-pore energy, $U(r)$, and this omission does not have an impact on the determination of Γ.

As the value of B is the same as discussed in section 3.1, U_b depends on the value of σ_t. With the increase of σ_t, U_b decreases and thus increases the rupture kinetics according to Eq (6). As

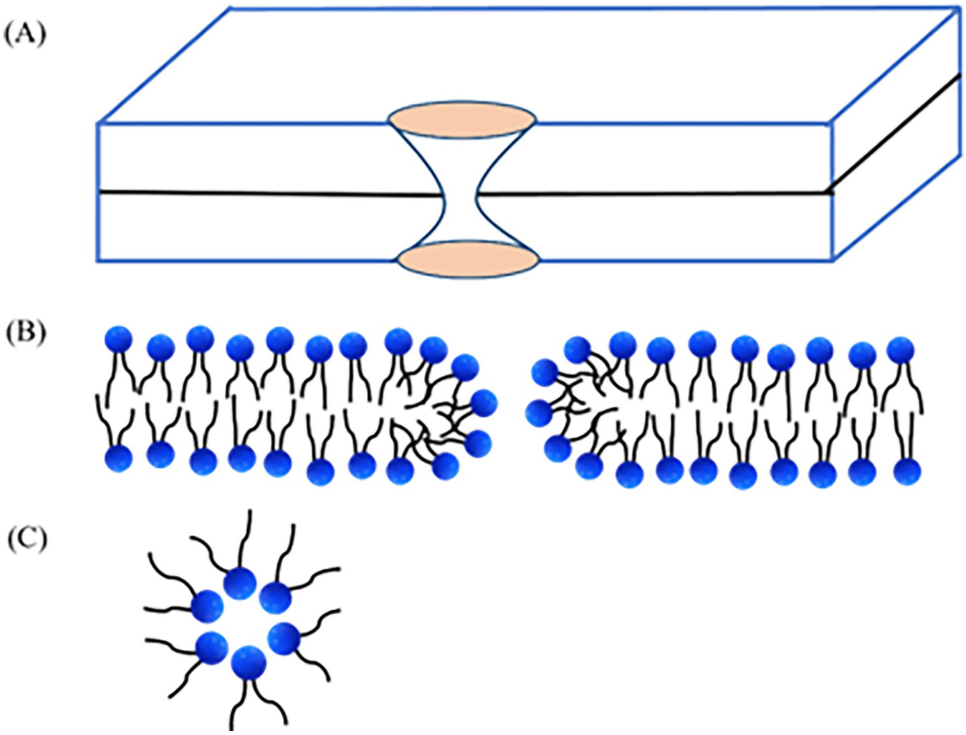

Fig 13. An illustration of a toroidal pore. (A) Total view, (B) side view, and (C) top view at the mid-plane of the lipid bilayer of a prepore.

https://doi.org/10.1371/journal.pone.0291496.g013

$\sigma_t = \sigma_e + \sigma_\varphi$, where, σ_e remains constant, σ_t depends onσ_φ, which is related to φ_m. The σ_e dependent kinetics of DOPG/DOPC/GrA (40/60/0.01)-GUVs in the presence of a fixed φ_m shows that σ_e increases the rupture of GUVs (Fig 6), which has a similar behavior of kinetics as observed in DOPG/DOPC (40/60)-GUVs. The increase in rupture events is attributed to the decrease in the energy barrier, as described by Eq (6).

In Figs 9 and 10, we observe stochastic rupture events in individual GUVs. This stochastic behavior indicates that the initiation of pore formation in lipid membranes is a random phenomenon. The time taken to reach the critical radius of a pore (r_c) varies among different GUVs. This random phenomenon has been observed in various cases [13,22,59]. For both HEPES and PIPES buffers, the rupture events, such as the rate constant and probability of rupture, increase with the applied σ_e. This is because higher σ_e reduces the energy barrier required to convert a prepore to a transmembrane pore, as described in Fig 7. The values of the rate constant and probability of rupture are relatively smaller in HEPES buffer compared to PIPES buffer (Fig 10). This difference can be attributed to the variations in salts and reagents present in these buffers, which can influence the kinetics of electroporation. The results obtained for electroporation kinetics in PIPES buffer closely matched the ones reported in a previous study [38]. The value of Γ for DOPG/DOPC (40/60)-GUVs in PIPES buffer is obtained $\Gamma = 10.4 \pm 0.9$ pN (Fig 11), which is well supported to the reported data such as $\Gamma = 10.7 \pm 0.4$ pN [31] and 11.5 pN [60].

The membrane potential of up to −90mV is created by subjecting the GUVs to an asymmetric distribution of K^+ in the buffer and to the addition of GrA in the bilayer. The method is in principle valid and this procedure has been employed before in the literature as we mentioned in section 2.3. It's important to ensure that everything is in place to effectively apply the Nernst equation and create the membrane potential. However, we couldn't conduct this specific investigation due to the required setup being unavailable. The present study involved various types of experiments, and the results were consistent with the previously reported findings, confirming the reliability of our research.

5. Conclusions

The electroporation of cell-mimetic lipid vesicles was studied under different membrane potentials, revealing interesting findings. It was observed that both the electroporation kinetics and the probability of rupture increased as the negative membrane potential was increased. Interestingly, the estimated pore edge tension remained relatively consistent across all the different membrane potentials tested. The addition of lateral tension due to applied electric field and the lateral tension due to membrane potential influences to decrease the barrier energy of the prepore, leading to increase the electroporation kinetics. This study presents a significant advancement in the field of electroporation technology, which holds great promise for various applications such as tumor and cancer cell ablation. Notably, this is the first reported investigation exploring the effects of membrane potential on electroporation. This study contributes to the expanding knowledge and applications of electroporation, offering new avenues for its utilization in the biomedical field.

Supporting information

S1 File. Suppl Infor_El_Pot_02.09.2023.
(PDF)

Author Contributions

Conceptualization: Md. Abdul Wadud, Mohammad Abu Sayem Karal, Md. Mamun Or Rashid.

Data curation: Md. Abdul Wadud, Mohammad Abu Sayem Karal.

Formal analysis: Md. Abdul Wadud, Mohammad Abu Sayem Karal, Md. Mamun Or Rashid.

Funding acquisition: Mohammad Abu Sayem Karal.

Investigation: Md. Abdul Wadud.

Methodology: Md. Abdul Wadud.

Project administration: Mohammad Abu Sayem Karal.

Supervision: Mohammad Abu Sayem Karal, Md. Mamun Or Rashid.

Validation: Md. Abdul Wadud, Mohammad Abu Sayem Karal, Md. Moniruzzaman, Md. Mamun Or Rashid.

Visualization: Md. Abdul Wadud.

Writing – original draft: Md. Abdul Wadud, Mohammad Abu Sayem Karal, Md. Moniruzzaman, Md. Mamun Or Rashid.

Writing – review & editing: Md. Abdul Wadud, Mohammad Abu Sayem Karal, Md. Moniruzzaman, Md. Mamun Or Rashid.

References

1. Chaffey N. Alberts B., Johnson A., Lewis J., Raff M., Roberts K., et al. Molecular biology of the cell. 4th edn. Ann Bot. 2003; 91: 401–401. https://doi.org/10.1093/aob/mcg023
2. Zaccolo M, Zerio A, Lobo MJ. Subcellular organization of the cAMP signaling pathway. Pharmacol Rev. 2021; 73: 278–309. https://doi.org/10.1124/pharmrev.120.000086 PMID: 33334857
3. Sundelacruz S, Levin M, Kaplan DL. Role of membrane potential in the regulation of cell proliferation and differentiation. Stem Cell Rev and Rep. 2009; 5: 231–246. https://doi.org/10.1007/s12015-009-9080-2 PMID: 19562527
4. Blackiston DJ, McLaughlin KA, Levin M. Bioelectric controls of cell proliferation: Ion channels, membrane voltage and the cell cycle. Cell Cycle. 2009; 8: 3527–3536. https://doi.org/10.4161/cc.8.21.9888 PMID: 19823012
5. Zhou Y, Wong C-O, Cho K, van der Hoeven D, Liang H, Thakur DP, et al. Membrane potential modulates plasma membrane phospholipid dynamics and K-Ras signaling. Science. 2015; 349: 873–876. https://doi.org/10.1126/science.aaa5619 PMID: 26293964
6. Richardson BD, Saha K, Krout D, Cabrera E, Felts B, Henry LK, et al. Membrane potential shapes regulation of dopamine transporter trafficking at the plasma membrane. Nat Commun. 2016; 7: 10423. https://doi.org/10.1038/ncomms10423 PMID: 26804245
7. Miller L, Leor J, Rubinsky B. Cancer cells ablation with irreversible electroporation. Technol Cancer Res Treat. 2005; 4: 699–705. https://doi.org/10.1177/153303460500400615 PMID: 16292891
8. Al-Sakere B, André F, Bernat C, Connault E, Opolon P, Davalos RV, et al. Tumor ablation with irreversible electroporation. PLOS ONE. 2007; 2: e1135. https://doi.org/10.1371/journal.pone.0001135 PMID: 17989772
9. Belehradek M, Domenge C, Luboinski B, Orlowski S, Belehradek J Jr., Mir LM. Electrochemotherapy, a new antitumor treatment. First clinical phase I-II trial. Cancer. 1993; 72: 3694–3700. https://doi.org/10.1002/1097-0142(19931215)72:12<3694::AID-CNCR2820721222>3.0.CO;2–2
10. Israelachvili JN. Electrostatic forces between surfaces in liquids. Intermolecular and surface forces. Elsevier; 2011. pp. 291–340. https://doi.org/10.1016/B978-0-12-375182-9.10014–4
11. Dimova R. Giant vesicles and their use in assays for assessing membrane phase state, curvature, mechanics, and electrical properties. Annu Rev Biophys. 2019; 48: 93–119. https://doi.org/10.1146/annurev-biophys-052118-115342 PMID: 30811220
12. Evans E, Smith BA. Kinetics of hole nucleation in biomembrane rupture. New J Phys. 2011; 13: 095010. https://doi.org/10.1088/1367-2630/13/9/095010 PMID: 21966242
13. Karal MAS, Ahamed MK, Ahmed M, Mahbub ZB. Recent developments in the kinetics of ruptures of giant vesicles under constant tension. RSC Adv. 2021; 11: 29598–29619. https://doi.org/10.1039/d1ra04647k PMID: 35479542
14. Cournia Z, Allen TW, Andricioaei I, Antonny B, Baum D, Brannigan G, et al. Membrane protein structure, function, and dynamics: a perspective from experiments and theory. J Membr Biol. 2015; 248: 611–640. https://doi.org/10.1007/s00232-015-9802-0 PMID: 26063070
15. Bamberg E, Läuger P. Channel formation kinetics of gramicidin A in lipid bilayer membranes. J Membr Biol. 1973; 11: 177–194. https://doi.org/10.1007/BF01869820 PMID: 4131309
16. Lundbæk JA, Collingwood SA, Ingólfsson HI, Kapoor R, Andersen OS. Lipid bilayer regulation of membrane protein function: gramicidin channels as molecular force probes. J R Soc Interface. 2009; 7: 373–395. https://doi.org/10.1098/rsif.2009.0443 PMID: 19940001
17. Shen J, Liu G, Han Y, Jin W. Artificial channels for confined mass transport at the sub-nanometre scale. Nat Rev Mater. 2021; 6: 294–312. https://doi.org/10.1038/s41578-020-00268-7
18. Kulbacka J, Choromańska A, Rossowska J, Weżgowiec J, Saczko J, Rols M-P. Cell membrane transport mechanisms: Ion channels and electrical properties of cell membranes. In: Kulbacka J, Satkauskas S, ed. Transport across natural and modified biological membranes and its implications in physiology and therapy. Cham: Springer Int Pub. 2017. pp. 39–58. https://doi.org/10.1007/978-3-319-56895-9_3 PMID: 28980039
19. Flood E, Boiteux C, Lev B, Vorobyov I, Allen TW. Atomistic simulations of membrane ion channel conduction, gating, and modulation. Chem Rev. 2019; 119: 7737–7832. https://doi.org/10.1021/acs.chemrev.8b00630 PMID: 31246417
20. Hossain F, Moghal MMR, Islam MZ, Moniruzzaman M, Yamazaki M. Membrane potential is vital for rapid permeabilization of plasma membranes and lipid bilayers by the antimicrobial peptide lactoferricin B. J Biol Chem. 2019; 294: 10449–10462. https://doi.org/10.1074/jbc.RA119.007762 PMID: 31118274

21. Rashid MMO, Moghal MMR, Billah MM, Hasan M, Yamazaki M. Effect of membrane potential on pore formation by the antimicrobial peptide magainin 2 in lipid bilayers. Biochim Biophys Acta (BBA)—Biomembr. 2020; 1862: 183381. https://doi.org/10.1016/j.bbamem.2020.183381 PMID: 32504547

22. Moghal MMR, Hossain F, Yamazaki M. Action of antimicrobial peptides and cell-penetrating peptides on membrane potential revealed by the single GUV method. Biophys Rev. 2020; 12: 339–348. https://doi.org/10.1007/s12551-020-00662-z PMID: 32152921

23. Keren K. Membrane tension leads the way. PNAS USA. 2011; 108: 14379–14380. https://doi.org/10.1073/pnas.1111671108 PMID: 21873200

24. Pontes B, Monzo P, Gauthier NC. Membrane tension: A challenging but universal physical parameter in cell biology. Semin Cell Dev Biol. 2017; 71: 30–41. https://doi.org/10.1016/j.semcdb.2017.08.030 PMID: 28851599

25. Barrau C, Teissié J, Gabriel B. Osmotically induced membrane tension facilitates the triggering of living cell electropermeabilization. Bioelectrochemistry. 2004; 63: 327–332. https://doi.org/10.1016/j.bioelechem.2003.11.009 PMID: 15110297

26. Zong W, Li Q, Zhang X, Han X. Deformation of giant unilamellar vesicles under osmotic stress. Colloids Surf B Biointerfaces. 2018; 172: 459–463. https://doi.org/10.1016/j.colsurfb.2018.08.053 PMID: 30196231

27. Brochard-Wyart F, de Gennes PG, Sandre O. Transient pores in stretched vesicles: role of leak-out. Phys A: Stat Mech Appl. 2000; 278: 32–51. https://doi.org/10.1016/S0378-4371(99)00559-2

28. Karatekin E, Sandre O, Guitouni H, Borghi N, Puech P-H, Brochard-Wyart F. Cascades of transient pores in giant vesicles: line tension and transport. Biophys J. 2003; 84: 1734–1749. https://doi.org/10.1016/S0006-3495(03)74981-9 PMID: 12609875

29. Levadny V, Tsuboi T, Belaya M, Yamazaki M. Rate constant of tension-induced pore formation in lipid membranes. Langmuir. 2013; 29: 3848–3852. https://doi.org/10.1021/la304662p PMID: 23472875

30. Leomil FSC, Zoccoler M, Dimova R, Riske KA. PoET: automated approach for measuring pore edge tension in giant unilamellar vesicles. Bioinfor Adv. 2021; 1: vbab037. https://doi.org/10.1093/bioadv/vbab037 PMID: 36700098

31. Tazawa K, Yamazaki M. Effect of monolayer spontaneous curvature on constant tension-induced pore formation in lipid bilayers. J Chem Phys. 2023; 158: 081101. https://doi.org/10.1063/5.0135561 PMID: 36859073

32. Moghal MMR, Islam MZ, Hossain F, Saha SK, Yamazaki M. Role of membrane potential on entry of cell-penetrating peptide transportan 10 into single vesicles. Biophys J. 2020; 118: 57–69. https://doi.org/10.1016/j.bpj.2019.11.012 PMID: 31810658

33. Hossain F, Dohra H, Yamazaki M. Effect of membrane potential on entry of lactoferricin b-derived 6-residue antimicrobial peptide into single Escherichia coli cells and lipid vesicles. J Bacteriol. 2021; 203: 10.1128/jb.00021-21. https://doi.org/10.1128/JB.00021-21 PMID: 33558393

34. Reeves JP, Dowben RM. Formation and properties of thin-walled phospholipid vesicles. J Cell Physiol. 1969; 73: 49–60. https://doi.org/10.1002/jcp.1040730108 PMID: 5765779

35. Tamba Y, Terashima H, Yamazaki M. A membrane filtering method for the purification of giant unilamellar vesicles. Chem Phys Lipids. 2011; 164: 351–358. https://doi.org/10.1016/j.chemphyslip.2011.04.003 PMID: 21524642

36. Feiner A-S, McEvoy AJ. The Nernst equation. J Chem Educ. 1994; 71: 493. https://doi.org/10.1021/ed071p493

37. Dimova R, Bezlyepkina N, Jordö MD, Knorr RL, Riske KA, Staykova M, et al. Vesicles in electric fields: Some novel aspects of membrane behavior. Soft Matter. 2009; 5: 3201. https://doi.org/10.1039/b901963d

38. Ahamed MK, Karal MAS, Ahmed M, Ahammed S. Kinetics of irreversible pore formation under constant electrical tension in giant unilamellar vesicles. Eur Biophys J. 2020; 49: 371–381. https://doi.org/10.1007/s00249-020-01440-1 PMID: 32494845

39. Litster JD. Stability of lipid bilayers and red blood cell membranes. Phys Lett A. 1975; 53: 193–194. https://doi.org/10.1016/0375-9601(75)90402-8

40. Kotnik T, Rems L, Tarek M, Miklavčič D. Membrane electroporation and electropermeabilization: mechanisms and models. Annu Rev Biophys. 2019; 48: 63–91. https://doi.org/10.1146/annurev-biophys-052118-115451 PMID: 30786231

41. Karal MAS, Levadnyy V, Tsuboi T, Belaya M, Yamazaki M. Electrostatic interaction effects on tension-induced pore formation in lipid membranes. Phys Rev E. 2015; 92. https://doi.org/10.1103/PhysRevE.92.012708 PMID: 26274204

42. Karal MAS, Orchi US, Towhiduzzaman M, Ahamed MK, Ahmed M, Ahammed S, et al. Electrostatic effects on the electrical tension-induced irreversible pore formation in giant unilamellar vesicles. Chem Phys Lipids. 2020; 231: 104935. https://doi.org/10.1016/j.chemphyslip.2020.104935 PMID: 32569600

43. Wohlert J, den Otter WK, Edholm O, Briels WJ. Free energy of a trans-membrane pore calculated from atomistic molecular dynamics simulations. J Chem Phys. 2006; 124: 154905. https://doi.org/10.1063/1.2171965 PMID: 16674263

44. Karal MAS, Levadnyy V, Yamazaki M. Analysis of constant tension-induced rupture of lipid membranes using activation energy. Phys Chem Chem Phys. 2016; 18: 13487–13495. https://doi.org/10.1039/c6cp01184e PMID: 27125194

45. Karal MAS, Ahamed MK, Rahman M, Ahmed M, Shakil MM, Rabbani KS. Effects of electrically-induced constant tension on giant unilamellar vesicles using irreversible electroporation. Eur Biophys J. 2019; 48: 731–741. https://doi.org/10.1007/s00249-019-01398-9 PMID: 31552440

46. Kulczycki A, Kajdas C, Kulczycki A, Kajdas C. A new attempt to better understand arrehnius equation and its activation energy. Tribology in Engineering. IntechOpen; 2013. https://doi.org/10.5772/54503

47. Weaver JC, Chizmadzhev YuA. Theory of electroporation: A review. Bioelectrochem Bioenerg. 1996; 41: 135–160. https://doi.org/10.1016/S0302-4598(96)05062-3

48. Montal M, Mueller P. Formation of bimolecular membranes from lipid monolayers and a study of their electrical properties. PNAS USA. 1972; 69: 3561–3566. https://doi.org/10.1073/pnas.69.12.3561 PMID: 4509315

49. Chen C, Smye SW, Robinson MP, Evans JA. Membrane electroporation theories: a review. Med Bio Eng Comput. 2006; 44: 5–14. https://doi.org/10.1007/s11517-005-0020-2 PMID: 16929916

50. Shibly SUA, Ghatak C, Karal MAS, Moniruzzaman M, Yamazaki M. Experimental estimation of membrane tension induced by osmotic pressure. Biophys J. 2016; 111: 2190–2201. https://doi.org/10.1016/j.bpj.2016.09.043 PMID: 27851942

51. Sarkar MK, Karal MAS, Ahmed M, Ahamed MK, Ahammed S, Sharmin S, et al. Effects of osmotic pressure on the irreversible electroporation in giant lipid vesicles. PLOS ONE. 2021; 16: e0251690. https://doi.org/10.1371/journal.pone.0251690 PMID: 33989363

52. Karal MAS, Alam JM, Takahashi T, Levadny V, Yamazaki M. Stretch-activated pore of the antimicrobial peptide, magainin 2. Langmuir. 2015; 31: 3391–3401. https://doi.org/10.1021/la503318z PMID: 25746858

53. Hasan M, Karal MAS, Levadnyy V, Yamazaki M. Mechanism of initial stage of pore formation induced by antimicrobial peptide magainin 2. Langmuir. 2018; 34: 3349–3362. https://doi.org/10.1021/acs.langmuir.7b04219 PMID: 29446954

54. Billah MM, Saha SK, Rashid MMO, Hossain F, Yamazaki M. Effect of osmotic pressure on pore formation in lipid bilayers by the antimicrobial peptide magainin 2. Phys Chem Chem Phys. 2022; 24: 6716–6731. https://doi.org/10.1039/d1cp05764b PMID: 35234764

55. Tieleman DP, Leontiadou H, Mark AE, Marrink S-J. Simulation of pore formation in lipid bilayers by mechanical stress and electric fields. J Am Chem Soc. 2003; 125: 6382–6383. https://doi.org/10.1021/ja029504i PMID: 12785774

56. Ring A. Gramicidin channel-induced lipid membrane deformation energy: influence of chain length and boundary conditions. Biochim Biophys Acta (BBA)—Biomembr. 1996; 1278: 147–159. https://doi.org/10.1016/0005-2736(95)00220-0 PMID: 8593271

57. Szule JA, Rand RP. The effects of gramicidin on the structure of phospholipid assemblies. Biophys J. 2003; 85: 1702–1712. https://doi.org/10.1016/S0006-3495(03)74600-1 PMID: 12944285

58. Ma Y, Poole K, Goyette J, Gaus K. Introducing membrane charge and membrane potential to T cell signaling. Front Immunol. 2017; 8: 1513. https://doi.org/10.3389/fimmu.2017.01513 PMID: 29170669

59. Islam MZ, Alam JM, Tamba Y, Karal MAS, Yamazaki M. The single GUV method for revealing the functions of antimicrobial, pore-forming toxin, and cell-penetrating peptides or proteins. Phys Chem Chem Phys. 2014; 16: 15752–15767. https://doi.org/10.1039/c4cp00717d PMID: 24965206

60. Evans E, Heinrich V, Ludwig F, Rawicz W. Dynamic tension spectroscopy and strength of biomembranes. Biophys J. 2003; 85: 2342–2350. https://doi.org/10.1016/S0006-3495(03)74658-X PMID: 14507698